Supporting Information

Multi-functional molecule interface modification for high-performance inverted wide-bandgap perovskite cells and modules

Yang Yang[a#], Qing Chang[c#], Yuyao Yang[a], Yuhui Jiang[a], Zhiyuan Dai[a], JiangWei Huo[a], Pengfei Guo[a], Xiaofeng Huang[c], Hui Shen[d], Zhe Liu[a], Ruihao Chen[a,b,e*] and Hongqiang Wang[a,b*]

a. State Key Laboratory of Solidification Processing, Center for Nano Energy Materials, School of Materials Science and Engineering, Northwestern Polytechnical University and Shaanxi Joint Laboratory of Graphene, Xi'an 710072, China

b. Chongqing Innovation Center, Northwestern Polytechnical University, Chongqing, 401135, China

c. College of Chemistry and Chemical Engineering, Xiamen University, Xiamen, 361005, China

d. College of Energy Material and Chemistry, Inner Mongolia University, Hohhot, 010021, China

e. Research & Development Institute of Northwestern Polytechnical University in Shenzhen, Shenzhen, 518063, China

** Corresponding authors.*

E-mail: rhchen@nwpu.edu.cn, hongqiang.wang@nwpu.edu.cn

Experimental Section

Materials

PbI_2, MAI, FAI, CsI and MABr were purchased from p-OLED. FTO (14 Ω sq^{-1}) and PCBM were purchased from AET and VIZUCHEM, respectively. MeO-2PACz, BCP, DMF, DMSO, EA, IPA and 2-Methoxyethanol were purchased from Sigma-Aldrich.

Synthesis of MHI molecule: 3-methyl-1-pyridin-6-ylmethyl-benzimidazolium chloride (MHI) was synthesized by reacting 1-methylbenzimidazole (5 mmol), 2-(chloromethyl) pyridine (1 mL) and K_2CO_3 (7 mmol) suspended in 30 mL CH_3CN, followed by refluxing and stirring. After two days, the mixture was dried up. The target product was extracted by excess CH_2Cl_2, followed by filtering. After removing the solvent, the product was isolated as while powder with the yield of 67%.

Device fabrication

The device configuration of FTO/MeO-2PACz/perovskite/MHI/PCBM/BCP/Ag were used, wherein the FTO was the bottom layer. The process for fabricating the device is summarized as follow: FTO substrate was washed and oxygen-plasma-treated referred to the previous work [1], MeO-2PACz solution (1 mg/mL in isopropanol) is spun on FTO substrate (4000 rpm for 30 s) and then annealed at 100 °C for 10 min. For depositing $Cs_{0.05}(FA_{0.77}MA_{0.23})_{0.95}Pb(I_{0.77}Br_{0.23})_3$ layer, a mixture solution of 0.05 mmol CsI, 1.09 mmol FAI, 0.32 mmol MABr, 1.14 mmol PbI_2, 0.35 mmol $PbBr_2$ and additives (200 μL of DMSO and excess 4.5 mol% of PbI_2) in 800 μL DMF is spun on FTO/MeO-2PACz substrates (3000 rpm for 30 s), and then 150 μL EA was dropped on above spinning substrate at 15 s prior the end of the process, and then the film was heat-treated at 120 °C for 20 min. The MHI/IPA solution (70 μL) was spun on the surface of perovskite film at 2000 rpm, and then heated on a 100 °C hot plate for 5 min. The subsequent deposition of PCBM, BCP and Ag layer was according to the previous works.[2] The active areas of the small device and minimodule were defined by the corresponding area masks.

For the fabrication of semi-transparent solar modules, the HTL layer, perovskite layer and ETL layer were according to the small-area device fabrication. As the top transparent electrode, 100 nm of ITO is sputtered using Angstrom EvoVac sputtering system after reaching a base pressure $<1\times10^{-6}$ Torr. For the P1-P2-P3 laser-patterning lines and the remaining process were according to the previous works.[3]

Characterization

The absorption of perovskite films was test by UV-vis spectrophotometer (Shimadzu UV-2550). Morphology of the films and devices was tested on a scanning electron microscope. The PL and TRPL (excitation at 510 nm) spectra were obtained using a Pico Quant Fluo Time 300 fluorescence spectrometer. Time-resolved femtosecond transient absorption spectroscopy (TAs) measurements were performed utilizing a commercial TA system.[4] The current–voltage (*J-V*) curves characteristics were measured under 100 mW/cm^2 (AM 1.5G illumination) calibrated by a certified reference solar cell in a Enli Technology solar simulator (IVS-KA5000) and a Keithley 2420 source/meter. The EQE spectra were measured by an Enli Technology EQE measurement system. Light stability test (ISOS-L-1I) was tested under the LED array solar simulator in N_2 glovebox. Transient photovoltage (TPV) and transient photocurrent (TPC) for PSCs were measured referred to the previous work.[5] The electrostatic potential (ESP) configuration of MHI and the calculation related to the interaction between Zn^{2+}/SO2- 4and molecules conducted in Dmol3 program. The structure optimization was performed at GGA/PBE level with DND basis set. The structure optimization was performed at GGA/PBE level with DND basis set. DFT Calculations: The $CsPbI_3$ model structure optimization and electronic density of states calculation are carried out by the density transmission theory of CASTEP, and the model is built through Materials Studio. The density functional selects the Perdew-Burke–Ernzerhof (PBE) function to perform the generalized gradient approximation calculation. The cut-off energy of plane wave is 500 eV, and the convergence tolerance of energy is 10^{-5} eV, and the maximum force is 10^{-4} eV Å^{-1}.

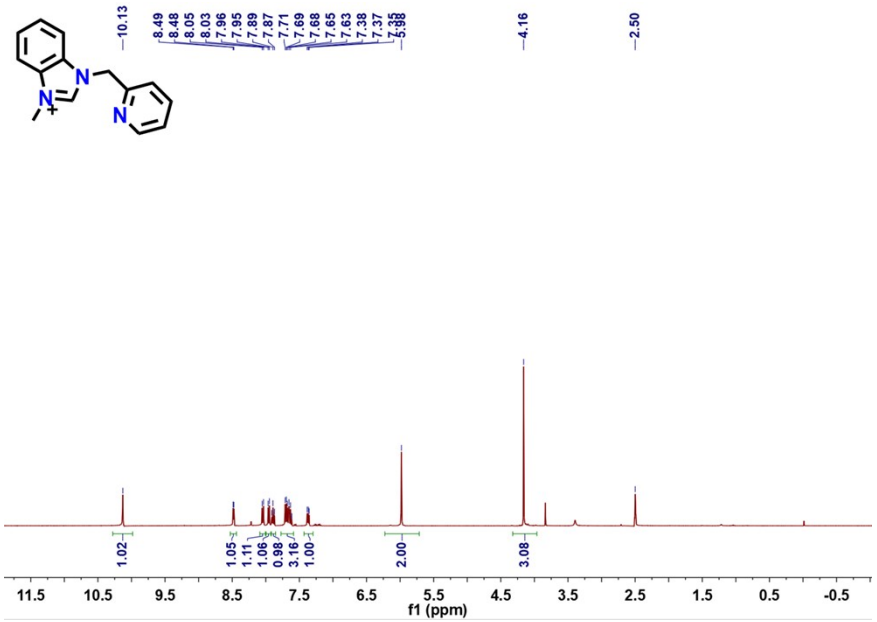

^{1}H NMR (400 MHz, DMSO-d_6) δ 10.13 (s), 8.48 (d, J = 4.8 Hz), 8.04 (d, J = 7.8 Hz), 7.96 (d, J = 7.7 Hz), 7.89 (t, J = 8.5 Hz), 7.77-7.59 (m), 7.43 - 7.30 (m), 5.98 (s), 4.16 (s).

Figure S1. ^{1}H NMR spectra of MHI powder dissolved in DMSO-d_6.

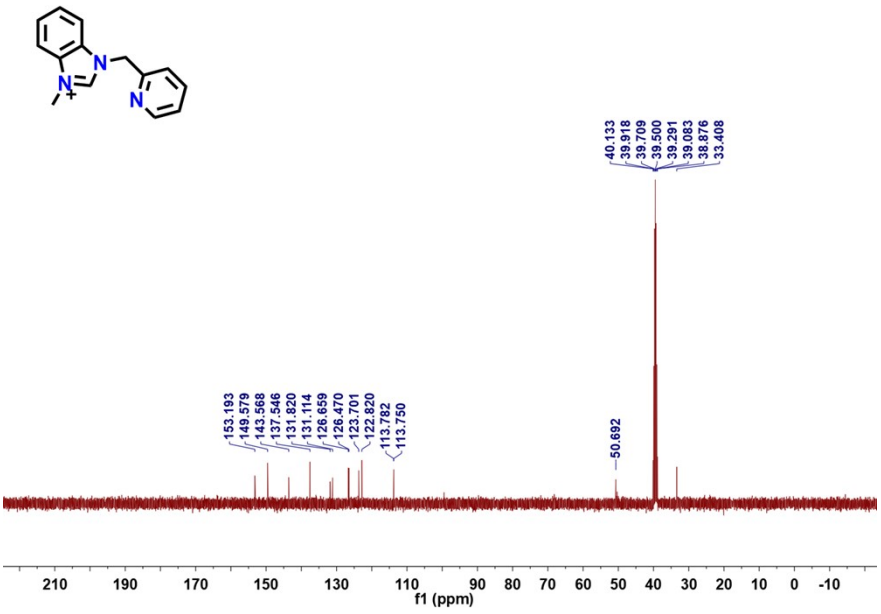

^{13}C NMR (101 MHz, DMSO-d_6) δ 143.57 (s), 140.13-138.50 (m), 137.25 - 133.63 (m), 130.90 - 128.54 (m), 126.56 (d, J = 19.0 Hz), 123.70 (s), 121.97 - 120.34 (m), 119.46 - 118.50 (m), 118.50 - 114.80 (m), 112.59 - 110.01 (m), 52.16 -51.89 (m), 51.89 - 51.77 (m), 51.72- 51.53 (m), 51.55 - 51.38 (m).

Figure S2. ^{13}C NMR spectra of MHI powder dissolved in DMSO-d_6.

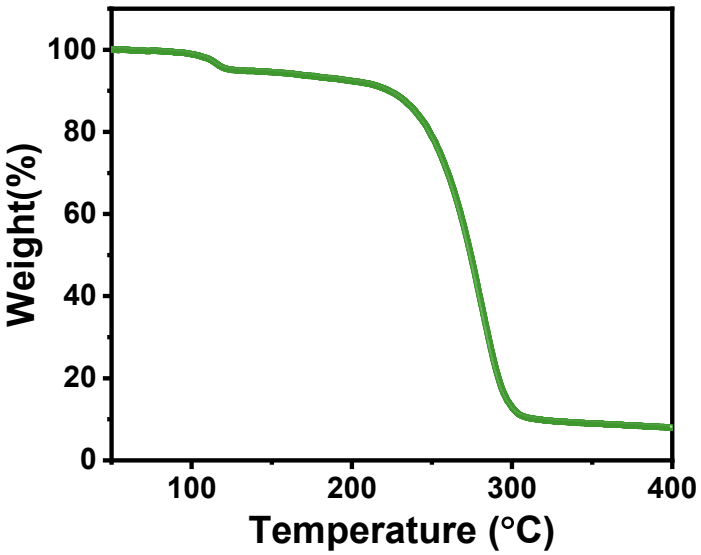

Figure S3. Thermogravimetric analysis (TGA) of MHI powder under N_2 atmosphere. The result demonstrated the MHI compound exhibits excellent thermal stability, but the initial weight loss occurred due to water molecule absorption during sample preparation and measurement.

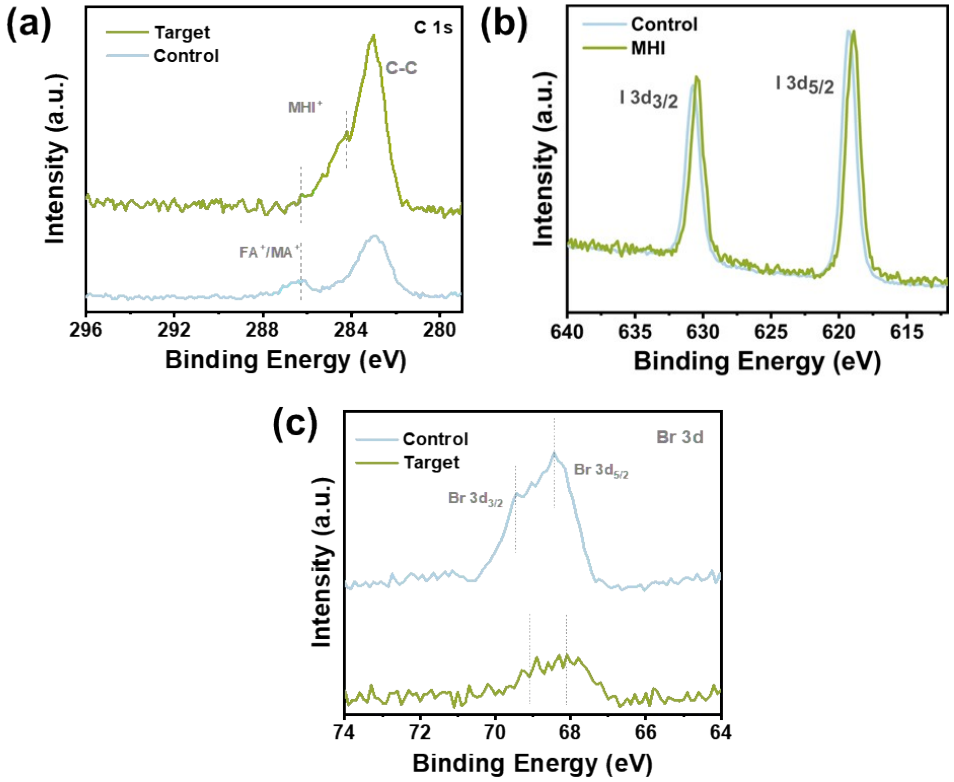

Figure S4. XPS spectra of (a) C 1s and (b) I 3d (c) Br 3d in the perovskite films with and without MHI.

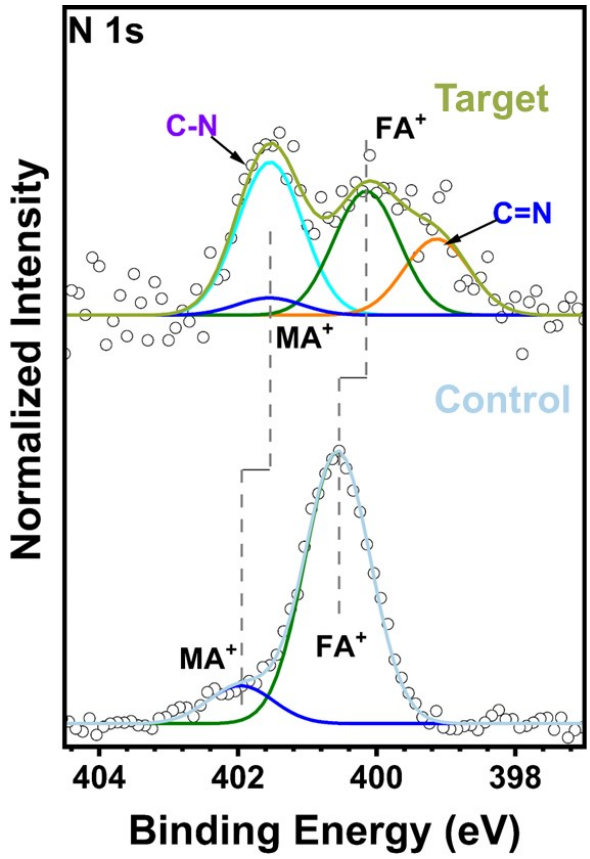

Figure S5. XPS spectra of N 1s in the perovskite films with and without MHI.

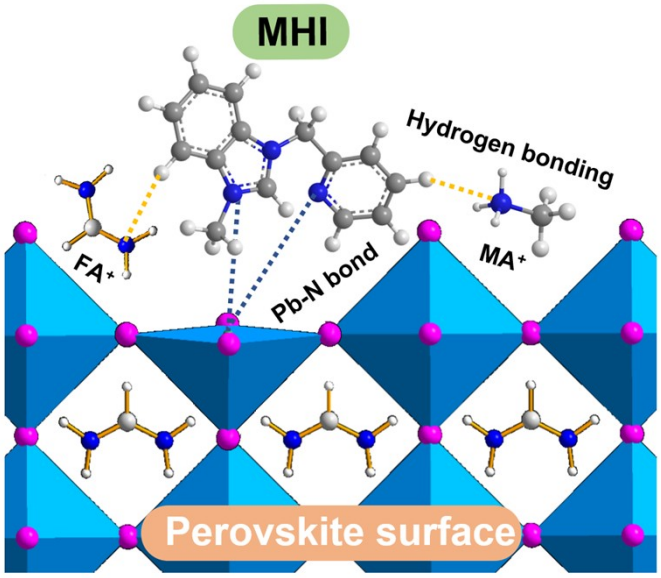

Figure S6. Illustration of the interaction models between MHI molecule and perovskite surface.

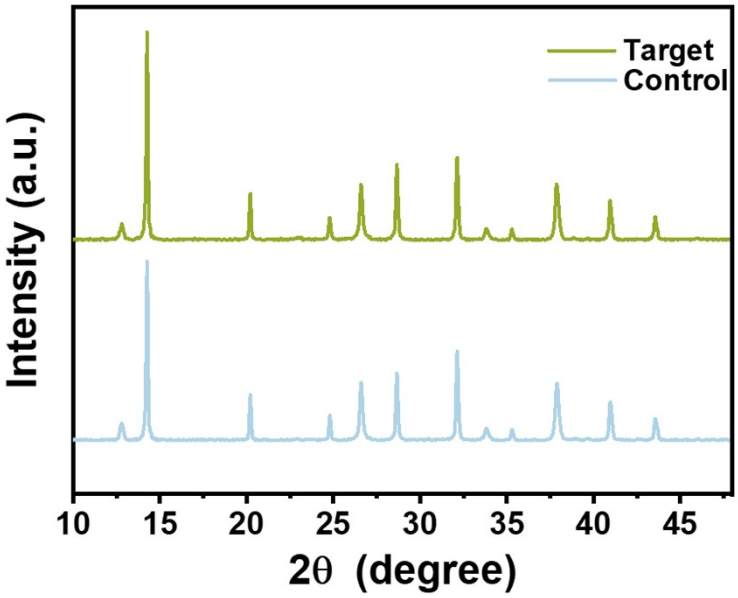

Figure S7. XRD patterns of the control and target perovskite films.

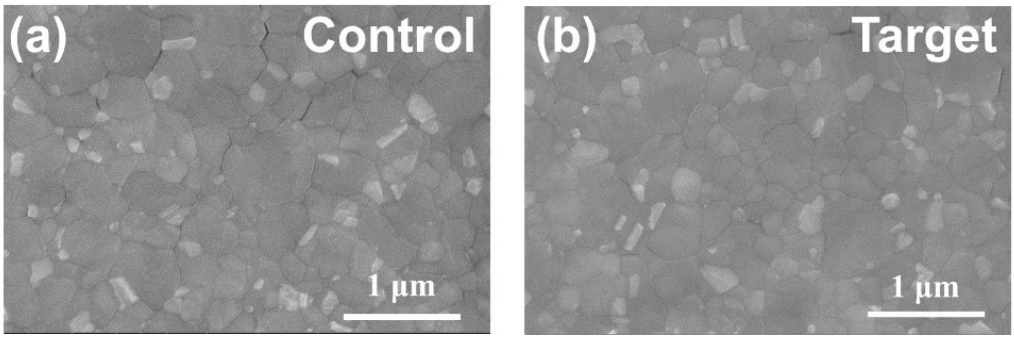

Figure S8. Top-view SEM images of the (a) control and (b) target perovskite films.

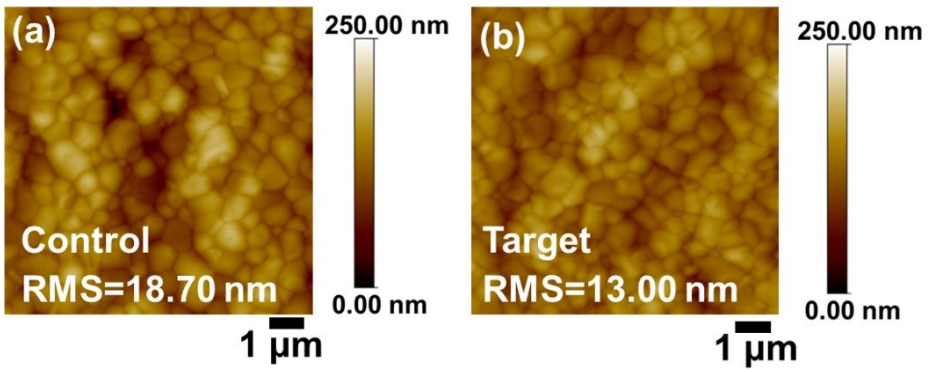

Figure S9. AFM characterization of the (a) control and (b) target perovskite films. RMS represents root mean square. and the root means square roughness (RMS) of the perovskite films without and with MHI is 18.70 nm and 13.00 nm, respectively.

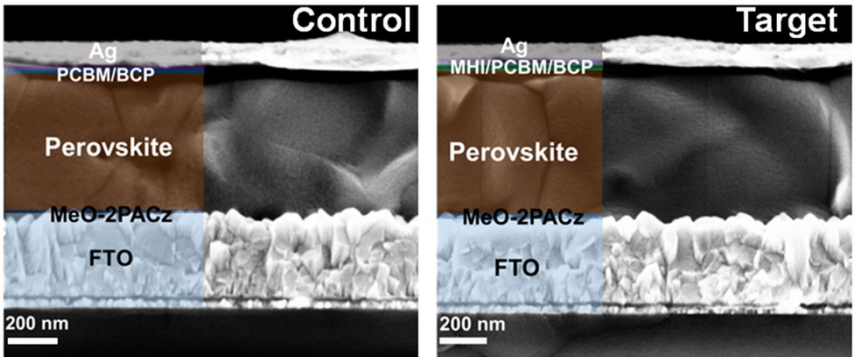

Figure S10. Cross-sectional SEM image of the control and target PSCs.

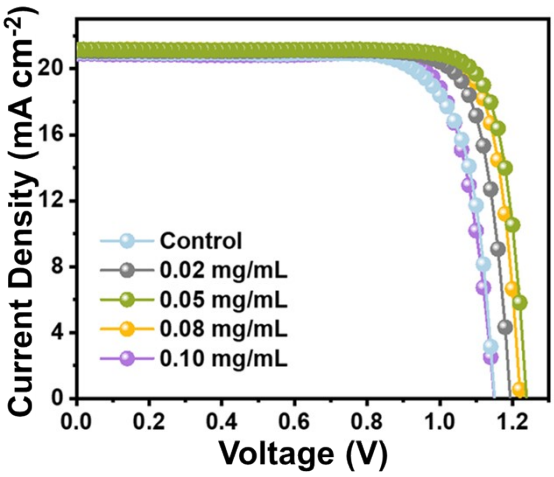

Figure S11. *J-V* curves of the perovskite films without and with MHI treatment in different concentrations.

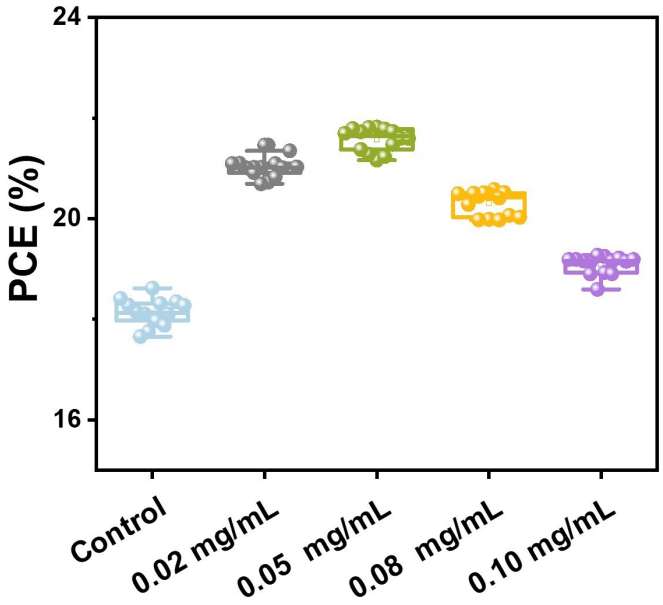

Figure S12. PCEs of distribution of 14 individual PSCs based on the perovskite films without and with MHI treatment in different concentrations. It is understandably that a small amount of MHI would lead to the insufficient modification of the surface for perovskites with low coverage, resulting the less obvious PCE improvement. However, the introduced excess MHI would act as insulating molecular capping layer and hinder the effective charges' extraction from the perovskite active layer, in turn reducing the device performance.

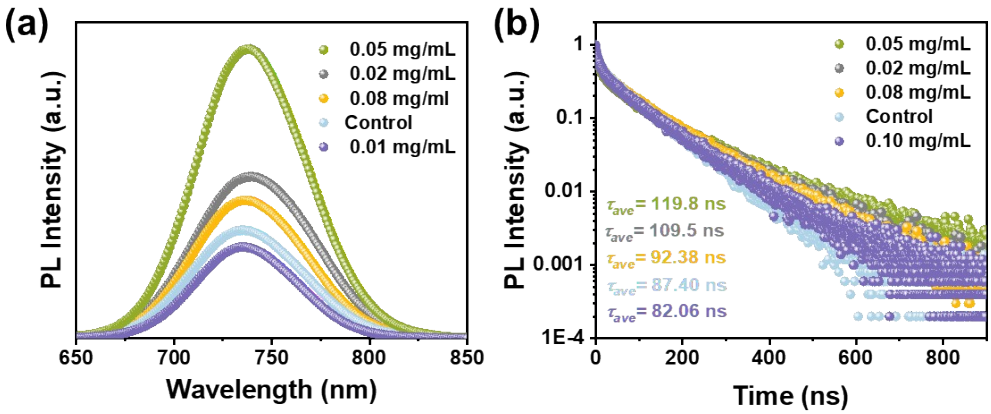

Figure S13. (a) PL and (b) TRPL spectra of the perovskite films without and with MHI treatment in different concentrations.

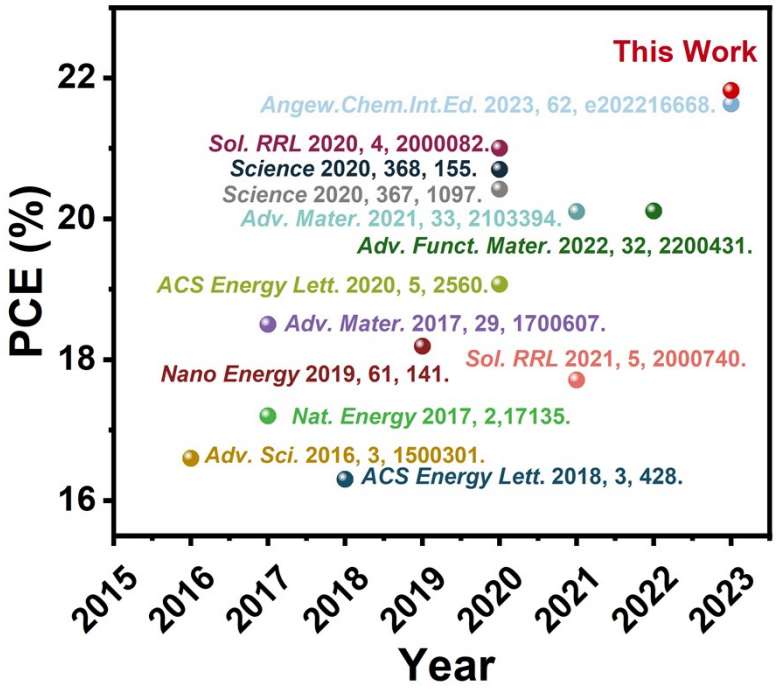

Figure S14. Summarized PCEs for the inverted wide-bandgap (1.66~1.72 eV) PSCs in the previous works.

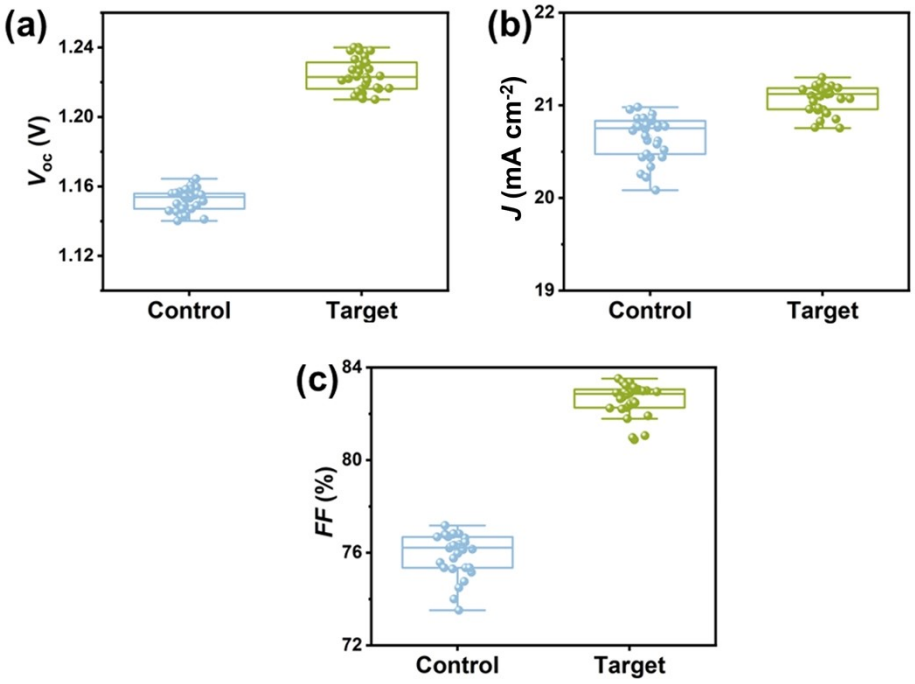

Figure S15. (a) V_{oc}, (b) current density (J) and (c) FF of Distribution of 30 individual PSCs based on the control and target perovskite films.

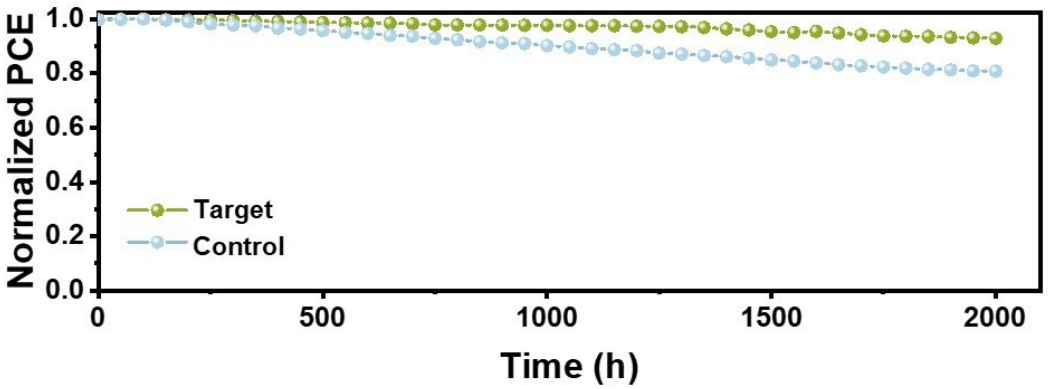

Figure S16. Moisture stability of the control and target PSCs under storage condition (25°C, 30% RH).

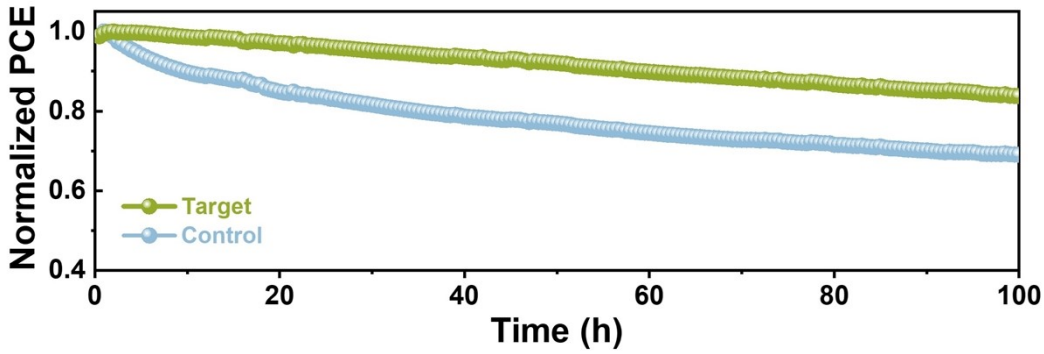

Figure S17. Light stability of the control and target PSCs under AM 1.5G irradiation in N_2 atmosphere.

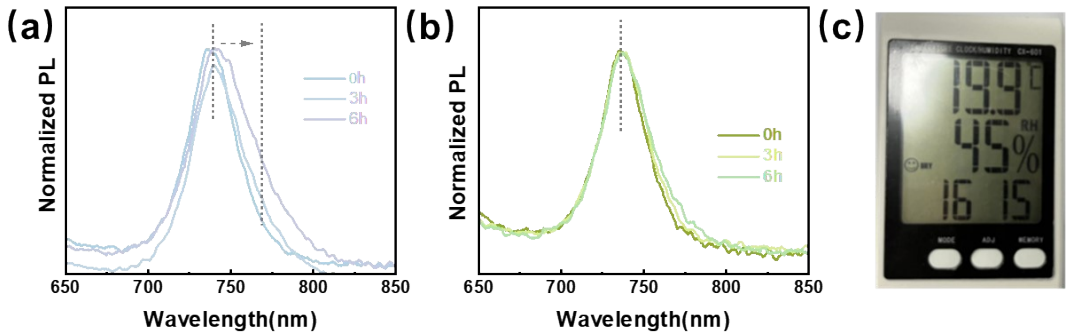

Figure S18. PL of the (a) control and (b) target perovskite films after different illumination times under AM 1.5G and 45% RH air condition. (c) Digital photo of hygrometer under the PL test condition.

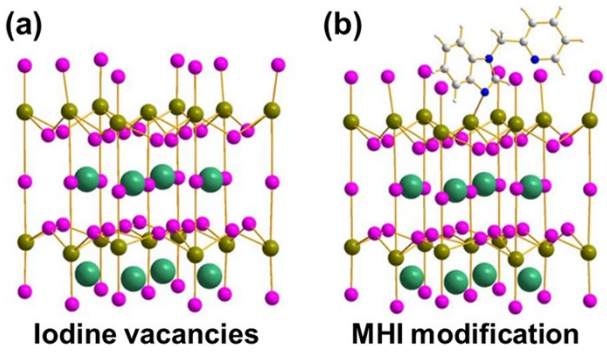

Figure S19. Scheme of the surface model of (a) control and (b) target perovskite films (purple ball is I, green ball is Cs, blue ball is nitrogen, brown ball is Pb, grey ball is C, white ball is H). The structure of $CsPbI_3$ acted as a model.

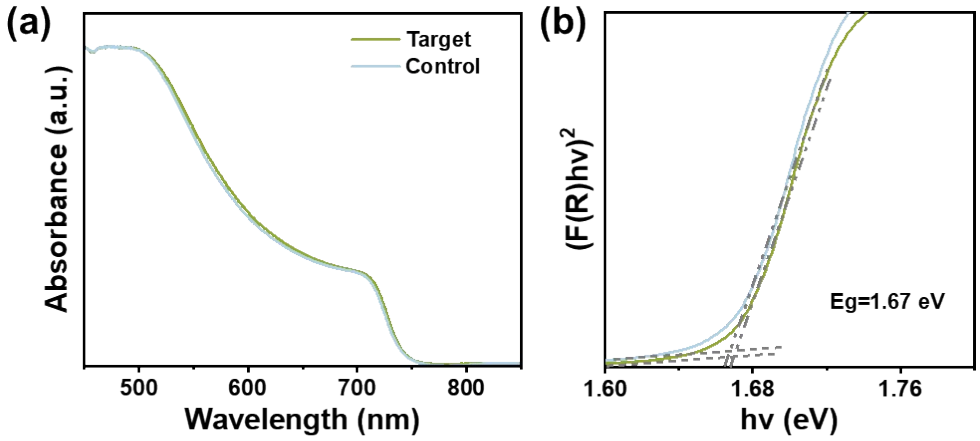

Figure S20. UV-vis absorption spectra (a) and the corresponding analyses (b) of perovskite films without (control) and with (target) MHI treatment.

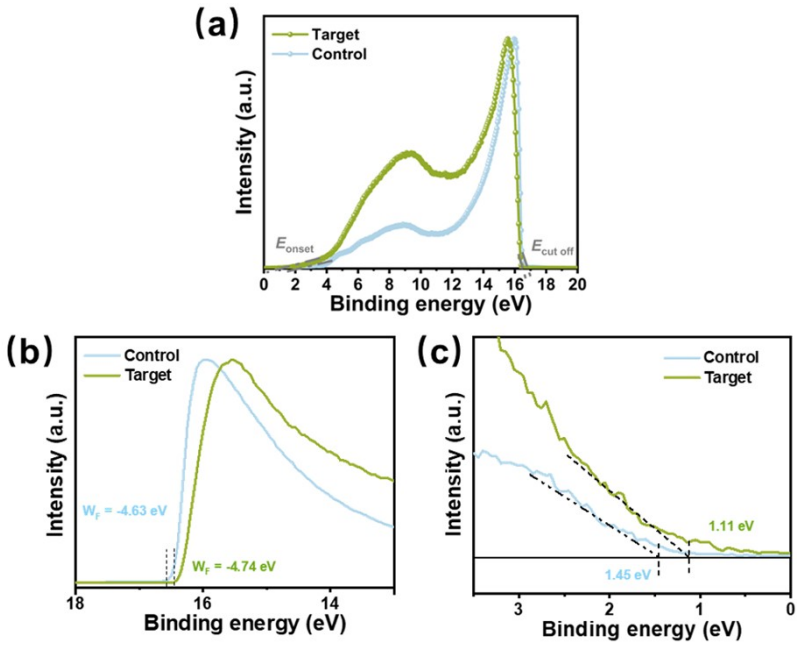

Figure S21. UPS spectra of the control and target perovskite films.

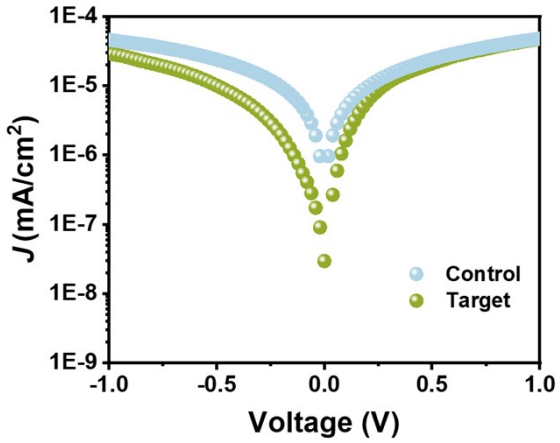

Figure S22. *J-V* curves of the control and target devices under dark condition.

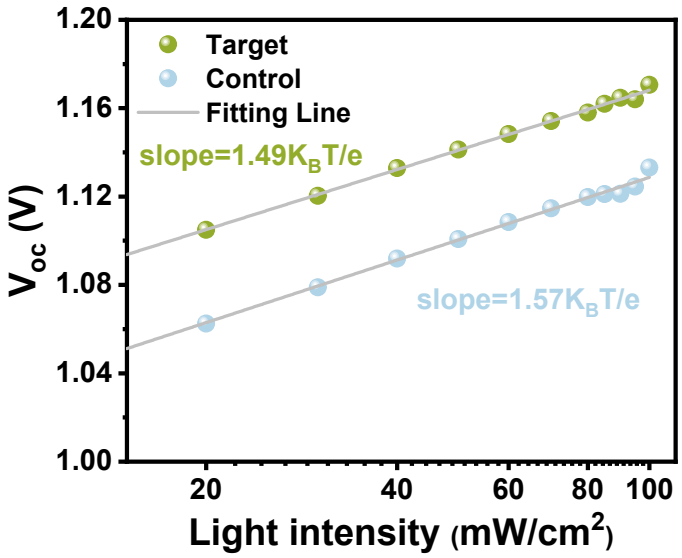

Figure S23. Dependence of V_{oc} at various light intensities for the control and target devices. At high kT/q ratios, the probability of trap-assisted recombination increases under open-circuit conditions. It is observed that the slope of the target device (1.49 kT/q) is lower than that of the control device (1.57 kT/q), indicating trap-assisted recombination is more efficiently hindered by MHI treatment.

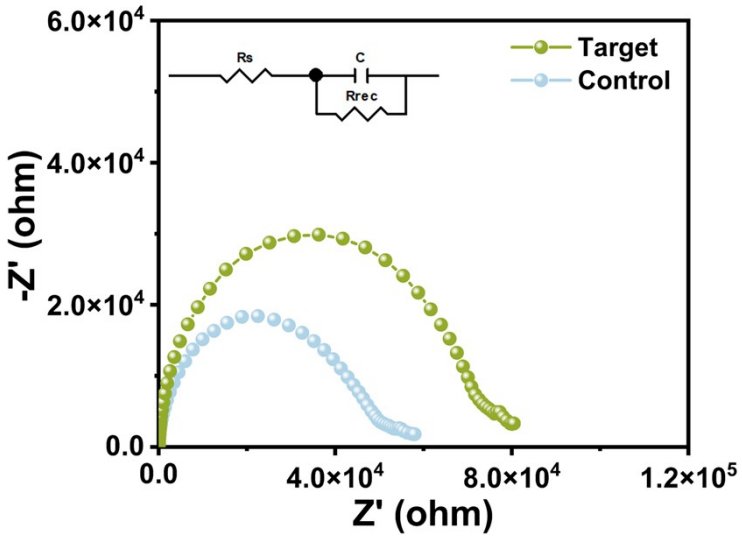

Figure S24. Nyquist plots of the control and target PSCs under dark conditions with a bias voltage of 1.05 V. The corresponding equivalent circuit consistsof series resistance (R_s) and recombination resistance (R_{rec}). The R_s and R_{rec} of the control device were 11.14 Ω and 827.90 Ω, while those of the target device were 9.28 Ω and 1228 Ω, respectively.

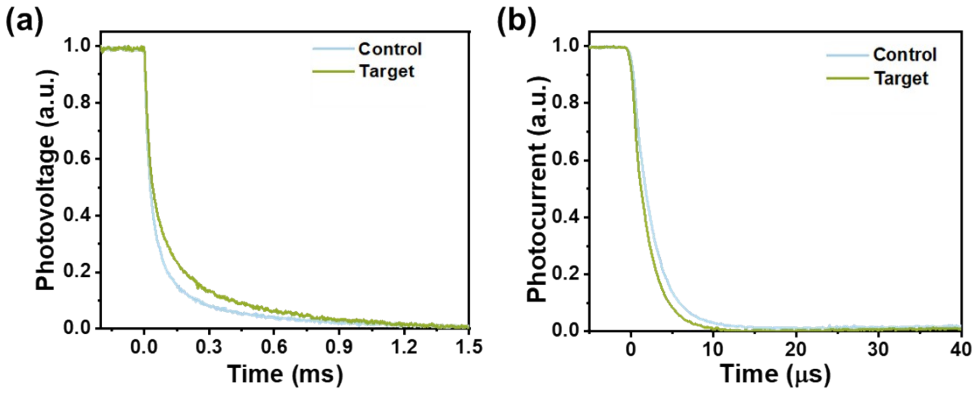

Figure S25. (a) TPV and (b) TPC decay curves of the control and target devices.

Table S1. Photovoltaic parameters of PSCs (0.05 cm^2 of active area).

Sample	V_{oc} (V)	J_{sc} (mA/cm^2)	FF (%)	PCE (%)
0.0 mg/mL (Control)	1.15	20.98	77.18	18.62
0.02 mg/mL	1.22	21.22	82.90	21.46
0.05 mg/mL (Target)	1.24	21.18	83.07	21.82
0.08 mg/mL	1.19	21.16	81.76	20.59
0.10 mg/mL	1.15	20.97	79.81	19.25

Table S2. Photovoltaic parameters of PSC modules (1.92 cm^2 of active area).

Sample	V_{oc} (V)	J_{sc} (mA/cm^2)	FF (%)	PCE (%)
Target	4.87	4.68	79.22	18.05
Control	4.77	4.62	75.63	16.67

References

[1] H. Chen, A. Maxwell, C. Li, S. Teale, B. Chen, T. Zhu, E. Ugur, G. Harrison, L. Grater, J. Wang, Z. Wang, L. Zeng, S. M. Park, L. Chen, P. Serles, R. A. Awni, B. Subedi, X. Zheng, C. Xiao, N. J. Podraza, T. Filleter, C. Liu, Y. Yang, J. M. Luther, S. De Wolf, M. G. Kanatzidis, Y. Yan and E. H. Sargent, *Nature*, 2022, **613**, 676-681.

[2] Y. Zheng, X. Wu, J. Liang, Z. Zhang, J. Jiang, J. Wang, Y. Huang, C. Tian, L. Wang, Z. Chen

and C. C. Chen, *Adv. Funct. Mater*, 2022, **32**, 2200431.

[3] R. Chen, Y. Wu, Y. Wang, R. Xu, R. He, Y. Fan, X. Huang, J. Yin, B. Wu, J. Li and N. Zheng, *Adv. Funct. Mater*, 2020, 31, 2008760.

[4] J. Liu, E. Aydin, J. Yin, M. De Bastiani, F. H. Isikgor, A. U. Rehman, E. Yengel, E. Ugur, G. T. Harrison, M. Wang, Y. Gao, J. I. Khan, M. Babics, T. G. Allen, A. S. Subbiah, K. Zhu, X. Zheng, W. Yan, F. Xu, M. F. Salvador, O. M. Bakr, T. D. Anthopoulos, M. Lanza, O. F. Mohammed, F. Laquai and S. De Wolf, *Joule*, 2021, **5**, 3169-3186.

[5] Y. Zhou, Y.-H. Jia, H.-H. Fang, M. A. Loi, F.-Y. Xie, L. Gong, M.-C. Qin, X.-H. Lu, C.-P. Wong and N. Zhao, *Adv. Funct. Mater.*, 2018, **28**, 1803130.